Pergamon

Int. J. Heat Mass Transfer. Vol. 40, No. 3, pp. 665–687, 1997

0017–9310/97 $15.00 + 0.00

PII: S0017–9310(96)00154–8

The unsteady penetration of free convection flows caused by heating and cooling flat surfaces in a porous media

R. BRADEAN and D. B. INGHAM
Department of Applied Mathematical Studies, The University of Leeds, Leeds LS2 9JT, U.K.

P. J. HEGGS
Department of Chemical Engineering, UMIST, Manchester M60 1QD, U.K.

and

I. POP
Faculty of Mathematics, The University of Cluj, R-3400 Cluj, CP 253, Romania

(*Received* 15 *December* 1995)

Abstract—Free convection flow is generated in a porous media adjacent to a vertical or horizontal flat surface which is suddenly heated and cooled, sinusoidally along its length. An approximate analytical solution, which is valid for small times and for any value of the Rayleigh number, *Ra*, is obtained by matching inner and outer expansions. A numerical solution is also obtained which matches the small time analytical solution to the ultimate steady-state solution when such a solution exists. In both configurations the flow pattern is that of a row of counter rotating cells situated close to the surface. When the surface is vertical and for $Ra \gtrsim 40$, two recirculating regions develop at small times at the point of collision of two boundary layers which flow along the surface. However, for $40 \lesssim Ra \lesssim 150$, the steady state solution, proposed by Bradean *et al.* [*International Journal of Heat and Mass Transfer*, 1996, **39**, 2545–2557], using additional symmetrical conditions is unstable and at very large time the solution is periodic in time. In the situation in which the surface is horizontal the collision of convection boundary layers occurs without separation. As time increases, the height of the cellular flow penetration increases and then decreases to its steady-state value. The heat penetrates infinitely into the porous media and the steady-state is approached later in time as the distance from the surface increases. Copyright © 1996 Elsevier Science Ltd.

1. INTRODUCTION

The development of supplementary energy resources, such as geothermal energy, has stimulated the study of convective flows through porous media. A very good and comprehensive review of the heat transfer mechanisms in geothermal systems has been performed by Cheng [1], containing many numerical and experimental simulations of convective flows through different geothermal reservoirs around the world with application to power generation and liquid waste disposal. The more recent book by Nield and Bejan [2] gathered many other studies of convection through porous media with application to irrigation systems, exploration of petroleum and gas fields, porous insulations and cooling of rotating electric windings.

In this paper the free convection fluid flow generated by an impulsively heated and cooled, in space, vertical or horizontal surface is considered. In the steady-state vertical configuration, Bradean *et al.* [3] showed that a cellular flow develops near the surface for small values of the Rayleigh number, *Ra*. However, for $40 \lesssim Ra \lesssim 150$, additional symmetrical conditions in the x direction must be assumed in order to obtain convergent numerical solutions, and two recirculating regions develop at the point of collision of the two boundary layers which flow along the surface, as postulated by Smith and Duck [4] for the problem of a rotating sphere in a fluid at rest.

Convergence of the numerical solution could not be obtained for $Ra \gtrsim 150$ and the evolution of the recirculating regions as the value of *Ra* increases implied that detachment occurs from the surface. In the horizontal situation, Poulikakos and Bejan [5] obtained steady-state numerical solutions using a prescribed temperature boundary condition at a large but finite distance from the surface. It was found that the cellular flow developed near the surface penetrates further into the porous media as *Ra* increases. However, Bradean *et al.* [6] showed analytically and numerically that the boundary condition of no heat transfer at an infinite distance from the surface is the appropriate physical boundary condition to enforce since the heat penetrates infinitely into the porous

NOMENCLATURE

c	constant, equation (61)
d	non-dimensional distance from the surface
D	solution domain
f	transformed streamfunction, equation (10)
g	acceleration due to gravity
K	permeability of the porous media
L	a characteristic length
$n_\xi+1$	number of nodal points in the ξ direction, equation (63)
$n_\eta+1$	number of nodal points in the η direction, equation (63)
$\tilde{N}u$	mean Nusselt number, equation (42) and (58)
P	constant, equation (19)
Q	average heat flux, equation (73)
Ra	Rayleigh number
t	non-dimensional time
T	non-dimensional temperature
u, v	non-dimensional velocity components in the x and y directions, respectively
$\tilde{u}$	mean fluid velocity, equations (41) and (57)
U_c	a characteristic velocity
x, y	non-dimensional Cartesian coordinates along and normal to the surface, respectively
$\tilde{z}$	transformed coordinate, equation (66).

Greek symbols

α	thermal diffusivity
β	coefficient of thermal expansion
ν	kinematic viscosity of the convective fluid
ψ	non-dimensional streamfunction
ξ	transformed coordinate, equation (10)
η	transformed coordinate, equation (61)
γ	constant, equation (7)
λ_1, λ_2	constants, equation (3).

Superscripts

$\hat{}$	dimensional variables
$\tilde{}$	scaled variables with the Rayleigh number, equation (7).

media. As the Rayleigh number increases, the height of the cellular flow penetration decreases whereas the temperature at infinity increases. The flow does not separate at the point of collision of the two boundary layers which flow along the horizontal surface and this was also obtained by Ingham *et al.* [7] in the situation in which the free convection boundary layers collide on a horizontal circular cylinder.

For impulsively started problems there are usually restrictions on the validity of the analytical and/or numerical solutions in time, see the analytical solutions obtained by Wang [8, 9] and Pop *et al.* [10, 11] using the method of matched asymptotic expansions and the numerical solutions obtained by Ingham *et al.* [7] and Collins and Dennis [12] using the numerical method of series truncation. However, numerical solutions which join the small and large time solutions have also been obtained by Ingham *et al.* [13] and Ingham and Brown [14].

In this study an analytical solution which is valid for small times is obtained using a matching technique in a similar way to that described by Wang [6, 7]. The method is presented in more detail by Bradean *et al.* [15, 16] and consists of obtaining expansions of the solution in terms of the small time inside and outside the thermal boundary-layer, which are then matched in order to take into account the outer flow from the thermal boundary-layer.

Finite-difference solutions are also obtained for small and large times and for different values of the Rayleigh number using the fully implicit Crank–Nicolson method. The prescribed constant temperature boundary condition is enforced at infinity by using a transformation in the direction normal to the surface as in the steady-state situations, see Bradean *et al.* [3, 6]. The appropriate scalings with the Rayleigh number and time are made at small times in the governing equations in order to take account of the growth of the thermal boundary-layer.

2. FORMULATION OF THE PROBLEM

A vertical horizontal surface is embedded in a porous media and initially the temperature, T_∞, is constant everywhere in space. Then at time $\hat{t} = 0$ the surface is impulsively heated and cooled, sinusoidally along its length, namely we have:

$$\hat{T} = T_a \sin(\hat{x}/L) + T_\infty \qquad \hat{t} \geqslant 0, \quad \hat{y} = 0, \quad -\infty < \hat{x} < \infty \qquad (1)$$

when the surface is vertical and

$$\hat{T} = T_a \cos(\hat{x}/L) + T_\infty \qquad \hat{t} \geqslant 0, \quad \hat{y} = 0, \quad -\infty < \hat{x} < \infty \qquad (2)$$

when the surface is horizontal, where the Cartesian coordinates $(\hat{x}, \hat{y})$ are chosen along and normal to the surface. It is assumed that the resulting flow is two-dimensional and the gravity, g, acts in the negative $\hat{x}$

or $\hat{y}$ direction depending on whether the surface is vertical or horizontal. Further, we assume Darcy's law and use the Boussinesq approximation. Then the non-dimensional governing equations can be written in terms of temperature, T, and streamfunction, ψ, see Nield and Bejan [2], as

$$\frac{\partial^2\psi}{\partial x^2}+\frac{\partial^2\psi}{\partial y^2}=-\lambda_1\frac{\partial T}{\partial x}+\lambda_2\frac{\partial T}{\partial y} \tag{3}$$

$$\frac{\partial T}{\partial t}+\frac{\partial\psi}{\partial y}\frac{\partial T}{\partial x}-\frac{\partial\psi}{\partial x}\frac{\partial T}{\partial y}=\frac{1}{Ra}\left(\frac{\partial^2 T}{\partial x^2}+\frac{\partial^2 T}{\partial y^2}\right) \tag{4}$$

where $(\lambda_1,\lambda_2)=(1,0)$ for the horizontal surface, $(\lambda_1,\lambda_2)=(0,1)$ for the vertical surface, $Ra=Kg\beta T_a L/(\nu\alpha)$ is the Rayleigh number and the velocities in the x and y directions are $u=\partial\psi/\partial y$ and $v=-\partial\psi/\partial x$, respectively. The non-dimensional variables are defined as follows:

$$x=\hat{x}/L,\quad y=\hat{y}/L,\quad u=\hat{u}/U_c,\quad v=\hat{v}/U_c \tag{5}$$

$$t=\hat{t}L/U_c,\quad T=(\hat{T}-T_\infty)/T_a,\quad \psi=\hat{\psi}(U_cL) \tag{6}$$

where $U_c=Kg\beta T_a/\nu$ is a characteristic speed.

A thermal boundary-layer is formed at small times adjacent to the surface and its thickness is proportional to $(t/Ra)^{1/2}$. Thus the variation of the solution with the Rayleigh number at small times is considered by using the following scalings:

$$y=\tilde{y}Ra^{-1/2},\quad \psi=\tilde{\psi}Ra^{-\gamma} \tag{7}$$

where $\gamma=1/2$ and $\gamma=1$ for the vertical and horizontal surfaces, respectively, and the governing equations (3) and (4) become

$$\frac{1}{Ra}\frac{\partial^2\tilde{\psi}}{\partial x^2}+\frac{\partial^2\tilde{\psi}}{\partial\tilde{y}^2}=-\lambda_1\frac{\partial T}{\partial x}-\lambda_2\frac{\partial T}{\partial\tilde{y}} \tag{8}$$

$$\frac{\partial T}{\partial t}+Ra^{1/2-\gamma}\left(\frac{\partial\tilde{\psi}}{\partial\tilde{y}}\frac{\partial T}{\partial x}-\frac{\partial\tilde{\psi}}{\partial x}\frac{\partial T}{\partial\tilde{y}}\right)=\frac{1}{Ra}\frac{\partial^2 T}{\partial x^2}+\frac{\partial^2 T}{\partial\tilde{y}^2}. \tag{9}$$

In order to take into account the growth of the thermal boundary-layer at small times, the further transformations

$$\tilde{y}=2t^{1/2}\xi,\quad \tilde{\psi}=(4t)^{\gamma}f(x,\xi,t) \tag{10}$$

are performed and equations (8) and (9) become

$$\frac{4t}{Ra}\frac{\partial^2 f}{\partial x^2}+\frac{\partial^2 f}{\partial\xi^2}=-\lambda_1\frac{\partial T}{\partial x}+\lambda_2\frac{\partial T}{\partial\xi} \tag{11}$$

$$\frac{\partial T}{\partial t}+\left(\frac{4t}{Ra}\right)^{\gamma-1/2}\left(\frac{\partial f}{\partial\xi}\frac{\partial T}{\partial x}-\frac{\partial f}{\partial x}\frac{\partial T}{\partial\xi}\right)=\frac{1}{Ra}\frac{\partial^2 T}{\partial x^2}+\frac{1}{4t}\left(\frac{\partial^2 T}{\partial\xi^2}+2\xi\frac{\partial T}{\partial\xi}\right). \tag{12}$$

It should be noted that at small times the thickness of the thermal boundary-layer does not depend on the inclination of the surface and this contrasts with the velocity scales which are different in the vertical and horizontal configurations.

At $t=0$, equations (11) and (12) for the temperature T_0 and the streamfunction, f_0, become:

$$\frac{\partial^2 T_0}{\partial\xi^2}+2\xi\frac{\partial T_0}{\partial\xi}=0 \tag{13}$$

$$\frac{\partial^2 f_0}{\partial\xi^2}=-\lambda_1\frac{\partial T_0}{\partial x}+\lambda_2\frac{\partial T_0}{\partial\xi} \tag{14}$$

which have to be solved subject to the boundary conditions

$$T_0=\lambda_1\cos(x)+\lambda_2\sin(x),\quad f_0=0 \quad \text{at } \xi=0,\quad 0\leqslant x\leqslant 2\pi \tag{15}$$

$$T_0\to 0,\quad \partial f_0/\partial\xi\to 0 \quad \text{as } \xi\to 0,\quad 0\leqslant x\leqslant 2\pi \tag{16}$$

and the solution is given by

$$T_0=\lambda_1\operatorname{erfc}(\xi)\cos(x)+\lambda_2\operatorname{erfc}(\xi)\sin(x) \tag{17}$$

$$f_0=\lambda_1\left[\tfrac{1}{2}(\xi^2+\tfrac{1}{2})\operatorname{erfc}(\xi)-2\pi^{-1/2}\xi\,e^{-\xi^2}-\tfrac{1}{4}\right]\sin(x)+\lambda_2\left[\xi\operatorname{erfc}(\xi)-\pi^{-1/2}(e^{-\xi^2}-1)\right]\sin(x). \tag{18}$$

Since the temperature along the surface in the x direction is 2π periodic, the solution domain for equations (11) and (12) is chosen to be

$$D=\{(x,\xi)\in\mathbb{R}\times\mathbb{R}: p\pi\leqslant x\leqslant(p+2)\pi,\quad 0\leqslant\xi<\infty\} \tag{19}$$

where, for convenience, we have taken $p=0$ for the vertical surface and $p=-1$ for the horizontal surface. Therefore, at small times, i.e. $0<t\leqslant t_p$, where t_p is a time to be specified, equations (11) and (12) have to be solved in the domain D subject to the initial conditions (17) and (18) and the following boundary conditions:

$$T(x,\xi)=\lambda_1\cos(x)+\lambda_2\sin(x),\quad f(x,\xi)=0 \quad \xi=0,\quad p\pi\leqslant x\leqslant(p+2)\pi \tag{20}$$

$$T(p\pi,\xi)=T((p+2)\pi,\xi),\quad f(p\pi,\xi)=f((p+2)\pi,\xi) \quad 0\leqslant\xi<\infty \tag{21}$$

$$T(x,\xi)\to 0,\quad \partial f/\partial\xi(x,\xi)\to 0 \quad \xi\to\infty,\quad p\pi\leqslant x\leqslant(p+2)\pi \tag{22}$$

for any $t\in(0,t_p)$. As time increases the thermal boundary-layer thickens and will only exist at large values of time when the Rayleigh number is very large. Thus, for times $t>t_p$, it is more convenient to solve equations (8) and (9) in the domain

$$\tilde{D}=\{(x,\tilde{y})\in\mathbb{R}\times\mathbb{R}: p\pi\leqslant x\leqslant(p+2)\pi,\quad 0\leqslant\tilde{y}<\infty\} \tag{23}$$

subject to the initial condition given by the solution

of equations (11) and (12) at $t = t_p$ and the boundary conditions

$$T(x,\tilde{y}) = \lambda_1 \cos(x) + \lambda_2 \sin(x), \quad \tilde{\psi}(x,\tilde{y}) = 0$$
$$\tilde{y} = 0, \quad p\pi \leqslant x \leqslant (p+2)\pi \tag{24}$$

$$T(p\pi,\tilde{y}) = T((p+2)\pi,\tilde{y}), \tag{25}$$
$$\tilde{\psi}(p\pi,\tilde{y}) = \tilde{\psi}((p+2)\pi,\tilde{y}) \quad 0 \leqslant \tilde{y} < \infty$$

$$T(x,\tilde{y}) \to 0, \quad \partial\tilde{\psi}/\partial\tilde{y}(x,\tilde{y}) \to 0$$
$$\tilde{y} \to \infty, \quad p\pi \leqslant x \leqslant (p+2)\pi \tag{26}$$

for any $t > t_p$.

In the steady-state vertical situation, Bradean *et al.* [3] could only obtain convergent numerical results for $40 \leqslant Ra \leqslant 150$ by considering additional symmetrical conditions in the x direction and hence the unsteady numerical solution may not converge to a steady-state for these values of the Rayleigh number. These conditions are therefore considered here in order to check the accuracy of the numerical method at large times, namely we look for solutions for which $T = 0$ and $\psi = 0$ at all planes $x = k\pi$, k integer. With this assumption, the temperature and the streamfunction are antisymmetric functions about the plane $x = \pi$, i.e. $T(x,y) = -T(2\pi - x, y)$ and $\psi(x,y) = -\psi(2\pi - x, y)$ for any $0 \leqslant x \leqslant \pi$ and $0 \leqslant y < \infty$ and at small times, i.e. $0 < t \leqslant t_p$, equations (11) and (12) now have to be solved in the domain

$$D_0 = \{(x,\xi) \in \mathbb{R} \times \mathbb{R} : 0 \leqslant x \leqslant \pi, \quad 0 \leqslant \xi < \infty\} \tag{27}$$

subject to the initial conditions (11) and the following boundary conditions

$$T(x,\xi) = \sin(x), \quad f(x,\xi) = 0 \quad \xi = 0, \quad 0 \leqslant x \leqslant \pi \tag{28}$$

$$T(x,\xi) = 0, \quad f(x,\xi) = 0 \quad x = 0, \quad 0 \leqslant \xi < \infty \tag{29}$$

$$T(x,\xi) \to 0, \quad \partial f/\partial\xi(x,\xi) \to 0 \quad \xi \to \infty, \quad 0 \leqslant x \leqslant \pi \tag{30}$$

for any $t \in (0, t_p)$. For larger values of time, i.e. $t > t_p$, the problem reduces to solving equations (8) and (9) in the domain

$$\tilde{D}_0 = \{(x,\tilde{y}) \in \mathbb{R} \times \mathbb{R} : 0 \leqslant x \leqslant \pi, \quad 0 \leqslant \tilde{y} < \infty\} \tag{31}$$

subject to the initial conditions given by the solution of equations (11) and (12) at $t = t_p$ and the boundary conditions

$$T(x,\tilde{y}) = \sin(x), \quad \tilde{\psi}(x,\tilde{y}) = 0 \quad \tilde{y} = 0, \quad 0 \leqslant x \leqslant \pi \tag{32}$$

$$T(x,\tilde{y}) = 0, \quad \tilde{\psi}(x,\tilde{y}) = 0 \quad x = 0, \pi, \quad 0 \leqslant \tilde{y} < \infty \tag{33}$$

$$T(x,\tilde{y}) \to 0, \quad \partial\tilde{\psi}/\partial\tilde{y}(x,\tilde{y}) \to 0 \quad \tilde{y} \to \infty, \quad 0 \leqslant x \leqslant \pi \tag{34}$$

for any $t > t_p$.

3. METHOD OF SOLUTION

An analytical solution, which is valid at small times and for any value of the Rayleigh number, is obtained using the matched asymptotic expansions technique. Finite-difference results are also presented for small and large times in the range of Rayleigh numbers $0 \leqslant Ra \leqslant 300$ for the vertical surface and $0 \leqslant Ra \leqslant 200/\pi$ for the horizontal surface.

3.1. *Analytical solution for small times*

Expansions of the temperature and the streamfunction in terms of the small time are obtained in an inner region, inside the thermal boundary-layer. However, this solution is not valid in the entire solution domain since there is an outer flow from the thermal boundary-layer and, therefore, an outer region, outside the thermal boundary-layer, has to be considered. In the outer region the temperature $T = 0$ and the flow is potential. In order to obtain the outer expansion of the streamfunction the boundary condition at $y = 0$ is found by comparing the inner and outer expansions in an intermediate region. By adding now the inner and outer solutions and subtracting the common part we obtain a solution which is valid over the entire solution domain. The composite expansions of the temperature, streamfunction, mean fluid velocity, $\tilde{u}$ and mean Nusselt number, $\tilde{Nu}$, along the surface are obtained, see Bradean *et al.* [15, 16], as follows.

(a) *Vertical surface.*

$$T = T_0 + T_1 t + 0(t^2) \tag{35}$$

$$f = f_0 + f_1 t + 0(t^2) \tag{36}$$

where

$$T_0 = \operatorname{erfc}(\xi)\sin(x) \tag{37}$$

$$T_1 = \frac{2}{Ra}(\xi^2 \operatorname{erfc}(\xi) - \pi^{-1/2}\xi e^{-\xi^2})\sin(x)$$
$$+ \left\{\frac{3\pi-4}{12\pi}[(2\xi^2+1)\operatorname{erfc}(\xi) - 2\pi^{-1/2}\xi e^{-\xi^2}]\right.$$
$$+ \frac{1}{4}(2\xi^2-1)\operatorname{erfc}^2(\xi) - \frac{3}{2}\pi^{-1/2}\xi e^{-\xi^2}\operatorname{erfc}(\xi)$$
$$\left. + \frac{1}{\pi}e^{-2\xi^2} - \frac{2}{3\pi}e^{-\xi^2}\right\}\sin(2x) \tag{38}$$

$$f_0 = [\xi \operatorname{erfc}(\xi) - \pi^{-1/2}(e^{-\xi^2} - e^{-y})] \sin(x) \quad (39)$$

$$f_1 = \frac{2}{Ra}\Bigg[\frac{1}{6}(4\xi^3 + 3\xi)\operatorname{erfc}(\xi) - \frac{1}{6}\pi^{-1/2}(4\xi^2 + 1)e^{-\xi^2} + \frac{1}{6}\pi^{-1/2}e^{-y}\Bigg]\sin(x) + \Bigg\{\frac{1}{12}(2\xi^3 - 3\xi)\operatorname{erfc}^2(\xi) - \frac{1}{12}\pi^{-1/2}(4\xi^2 - 11)e^{-\xi^2}\operatorname{erfc}(\xi) - \frac{4}{3}(2\pi)^{-1/2}\operatorname{erfc}(\sqrt{2}\xi) + \frac{1}{3}\Bigg[\frac{3\pi - 4}{12\pi}(2\xi^3 + 3\xi) + \pi^{-1/2}\Bigg]\operatorname{erfc}(\xi) - \frac{3\pi - 4}{18\pi}\Bigg[\pi^{-1/2}\xi^2 - \frac{3}{3\pi - 4}\xi + \pi^{-1/2}\Bigg]e^{-\xi^2} - \frac{(39 - 24\sqrt{2})\pi + 8}{36\pi} \times \pi^{-1/2}e^{-2y}\Bigg\}\sin(2x) \quad (40)$$

and

$$\tilde{u} = \int_0^{\pi} (\partial\tilde{\psi}/\partial\tilde{y})_{y=0}\, dx = 2 - 4(\pi Ra)^{-1/2}t^{1/2} + 2Ra^{-1}t - \tfrac{4}{3}\pi^{-1/2}Ra^{-3/2}t^{3/2} + 0(t^2) \quad (41)$$

$$\tilde{Nu} = \int_0^{\pi} (-\partial T/\partial\tilde{y})_{y=0}\, dx = 2^{-1}t^{-1/2}[4\pi^{-1/2} + 4\pi^{-1/2}Ra^{-1}t + 0(t^2)]. \quad (42)$$

(b) *Horizontal surface.*

$$T = T_0 + T_1 t^{1/2} + T_2 t + T_3 t^{3/2} + 0(t^2) \quad (43)$$

$$f = f_0 + f_1 t^{1/2} + f_2 t + f_3 t^{3/2} + 0(t^2) \quad (44)$$

where

$$T_0 = \operatorname{erfc}(\xi)\cos(x) \quad (45)$$

$$T_1 = 0 \quad (46)$$

$$T_2 = \frac{2}{Ra}[\xi^2 \operatorname{erfc}(\xi) - \pi^{-1/2}\xi e^{-\xi^2}]\cos(x) \quad (47)$$

$$T_3 = 4Ra^{-1/2}[h_1(\xi) + h_2(\xi)\cos(2x)] \quad (48)$$

$$f_0 = [(\tfrac{1}{2}\xi^2 + \tfrac{1}{4})\operatorname{erfc}(\xi) - \tfrac{1}{2}\pi^{-1/2}\xi e^{-\xi^2} - \tfrac{1}{4}e^{-y}]\sin(x) \quad (49)$$

$$f_1 = 0 \quad (50)$$

$$f_2 = \frac{2}{Ra}\Bigg[\Bigg(\frac{1}{6}\xi^4 + \frac{1}{4}\xi^2\Bigg)\operatorname{erfc}(\xi) - \frac{1}{6}\pi^{-1/2}(\xi^3 + \xi)e^{-\xi^2}\Bigg]\sin(x) \quad (51)$$

$$f_3 = h_3^*(\xi)\sin(2x) \quad (52)$$

where

$$h_1(\xi) = -\Bigg(\frac{1}{3}\xi^3 + \frac{1}{4}\xi\Bigg)\operatorname{erfc}^2(\xi) + \frac{1}{12}\pi^{-1/2}\Bigg(7\xi^2 + \frac{5}{2}\Bigg)e^{-\xi^2}\operatorname{erfc}(\xi) - \frac{1}{4\pi}\xi e^{-2\xi^2} + \frac{1}{16}\pi^{-1/2}e^{-\xi^2} + \frac{13}{48}\Bigg(\xi^3 + \frac{3}{2}\xi\Bigg)\operatorname{erfc}(\xi) - \frac{13}{48}\pi^{-1/2}(\xi^2 + 1)e^{-\xi^2}. \quad (53)$$

$h_2(\xi)$ is the solution of equation

$$\frac{d^2h_2}{d\xi^2} + 2\xi\frac{dh_2}{d\xi} - 6h_2 = \xi\operatorname{erfc}^2(\xi) + \pi^{-1/2}\Bigg(\xi^2 - \frac{1}{2}\Bigg)e^{-\xi^2}\operatorname{erfc}(\xi) - \frac{1}{\pi}\xi e^{-2\xi^2} - \frac{1}{2}\pi^{-1/2}e^{-\xi^2} \quad (54)$$

subject to homogeneous boundary conditions, namely

$$h_2(\xi) = 0 \quad \text{at } \xi = 0 \quad (55)$$

$$h_2(\xi) \to 0 \quad \text{as } \xi \to \infty. \quad (56)$$

$h_3^*(\xi)$ is obtained by matching with the fourth-order outer flow and

$$\tilde{u} = \int_0^{\pi} (\partial\tilde{\psi}/\partial\tilde{y})_{y=0}\, dx = -4\pi^{-1/2}t^{1/2} + 2Ra^{-1/2}t - \frac{4}{3Ra}\pi^{-1/2}t^{3/2} + 0(t^{5/2}) \quad (57)$$

$$\tilde{Nu} = \int_0^{\pi/2} (-\partial T/\partial\tilde{y})_{y=0}\, dx = \pi^{-1/2}t^{-1/2} + \frac{1}{Ra}\pi^{-1/2}t^{1/2} + Ra^{-1/2}\Bigg(\frac{2}{3} - \frac{5\pi}{32}\Bigg)t + 0(t^{3/2}). \quad (58)$$

3.2. *Numerical solution*

In order to enforce the boundary condition of no flow and zero temperature at infinity the solution domain D is divided into a finite region

$$D_a = \{(x,\xi)\in\mathbb{R}\times\mathbb{R}: p\pi \leqslant x \leqslant (p+2)\pi, \quad 0 \leqslant \xi \leqslant d\} \tag{59}$$

and a semi-infinite region

$$D_b = \{(x,\xi)\in\mathbb{R}\times\mathbb{R}: p\pi \leqslant x \leqslant (p+2)\pi, \quad d \leqslant \xi < \infty\} \tag{60}$$

which is then transformed using the scaling

$$\eta = 1 - \frac{1}{1+c(\xi-d)} \tag{61}$$

into the finite domain

$$D_c = \{(x,\eta)\in\mathbb{R}\times\mathbb{R}: p\pi \leqslant x \leqslant (p+2)\pi, \quad 0 \leqslant \eta \leqslant 1\}. \tag{62}$$

The constant $d > 0$ is chosen for the numerical solution to be independent of the value of d, whereas the parameter c has to be determined so as to match the grid systems in the domains D_a and D_c, namely

$$c = \frac{n_\xi}{d(n_\eta - 1)} \tag{63}$$

where $n_\xi + 1$ and $n_\eta + 1$ are the number of grid points taken in the ξ and η directions, respectively.

Thus, at small times, i.e. $0 < t \leqslant t_p$, equations (11) and (12) are solved in the domain D_a and the transformed equations

$$\frac{4t}{Ra}\frac{\partial^2 f}{\partial x^2} + c^2(1-\eta)^4\frac{\partial^2 f}{\partial \eta^2} - 2c^2(1-\eta)^3\frac{\partial f}{\partial \eta} = -\lambda_1\frac{\partial T}{\partial x} + \lambda_2 c(1-\eta)^2\frac{\partial T}{\partial \eta} \tag{64}$$

$$\frac{\partial T}{\partial t} + c(1-\eta)^2\left(\frac{4t}{Ra}\right)^{\gamma-1/2}\left(\frac{\partial f}{\partial \eta}\frac{\partial T}{\partial x} - \frac{\partial f}{\partial x}\frac{\partial T}{\partial \eta}\right) = \frac{1}{Ra}\frac{\partial^2 T}{\partial x^2} + \frac{1}{4t}\left\{c^2(1-\eta)^4\frac{\partial^2 T}{\partial \eta^2} - 2c^2(1-\eta)^3\frac{\partial T}{\partial \eta} + 2[cd(1-\eta)^2 + \eta(1-\eta)]\frac{\partial T}{\partial \eta}\right\} \tag{65}$$

are solved in the domain D_c subject to the initial condition (17) and (18) and the boundary conditions (20)–(22). At larger values of time, i.e. $t > t_p$, the transformation (61) is now used in the $\tilde{y}$ direction, namely

$$\tilde{z} = 1 - \frac{1}{1+c(\tilde{y}-d)} \tag{66}$$

and the problem reduces to solving equations (8) and (9) in the domain

$$\tilde{D}_a = \{(x,\tilde{y})\in\mathbb{R}\times\mathbb{R}: p\pi \leqslant x \leqslant (p+2)\pi, \quad 0 \leqslant \tilde{y} \leqslant d\} \tag{67}$$

and the transformed equations

$$\frac{1}{Ra}\frac{\partial^2\tilde{\psi}}{\partial x^2} + c^2(1-\tilde{z})^4\frac{\partial^2\tilde{\psi}}{\partial \tilde{z}^2} - 2c^2(1-\tilde{z})^3\frac{\partial\tilde{\psi}}{\partial\tilde{z}} = -\lambda_1\frac{\partial T}{\partial x} + \lambda_2 c(1-\tilde{z})^2\frac{\partial T}{\partial\tilde{z}} \tag{68}$$

$$\frac{\partial T}{\partial t} + c(1-\tilde{z})^2 Ra^{1/2-\gamma}\left(\frac{\partial\tilde{\psi}}{\partial\tilde{z}}\frac{\partial T}{\partial x} - \frac{\partial\tilde{\psi}}{\partial x}\frac{\partial T}{\partial\tilde{y}}\right) = \frac{1}{Ra}\frac{\partial^2 T}{\partial x^2} + c^2(1-\tilde{z})^4\frac{\partial^2 T}{\partial\tilde{z}^2} - 2c^2(1-\tilde{z})^3\frac{\partial T}{\partial\tilde{z}} \tag{69}$$

in the domain

$$\tilde{D}_c = \{(x,\tilde{z})\in\mathbb{R}\times\mathbb{R}: p\pi \leqslant x \leqslant (p+2)\pi, \quad 0 \leqslant \tilde{z} \leqslant 1\} \tag{70}$$

subject to the initial condition given by the solution of equations (11), (12), (64) and (65) at $t = t_p$ and the boundary conditions (24)–(26).

In the situation in which the surface is vertical and for $40 \leqslant Ra \leqslant 300$, the additional symmetrical conditions assumed in the steady-state by Bradean *et al.* [3] are also considered and a numerical solution in the domain D_0 is obtained in a similar way to that described above in the domain D.

Finite-difference results have been obtained using a fully implicit Crank–Nicolson method. The successive over relaxation method is then used to solve the resulting nonlinear system of algebraic equations iteratively at each time step. At each time step the iterative procedure is terminated when the maximum difference between two successive iterations of the temperature and streamfunction becomes less than a preassigned value, say 10^{-6}. However, at small times, i.e. $0 < t \leqslant t_p$, we were unable to obtain a convergent numerical solutions of the full equations (11) and (12) in the domain D and the temperature at large distances from the surface tends to infinity as the number of iterations increases. This is most likely to have been caused by the accuracy of the computer which in the iterative procedure cannot adequately deal with the term $\xi\,\partial T/\partial\xi$ for large values of ξ and small values of $\partial T/\partial\xi$. However, at small times the thermal boundary-layer is of thickness 0(1) in the domain D and therefore the temperature and the temperature gradient should be approximately zero in the domain D_c if the value of d chosen is sufficiently large. The difficulty can be overcome by neglecting the term $\xi\,\partial T/\partial\xi$ for large values of ξ in the energy equation, i.e. we neglect the term

$$A = 2[cd(1-\eta)^2 + \eta(1-\eta)]\frac{\partial T}{\partial\eta} \tag{71}$$

on the right hand side of equation (65) in the domain D_c. The result is that convergent numerical solution can now be obtained which satisfy the hypothesis that A is approximately zero everywhere in the domain D_c. At larger values of time, i.e. $t > t_p$, the full equations

(8) and (9) are solved in the domain $\tilde{D}$. It is now convenient to choose $t_p = 1/4$ since then

$$\tilde{y} = \xi, \quad \tilde{\psi}(x, \tilde{y}, t_p) = f(x, \xi, t_p) \tag{72}$$

and a value of $d = 2\pi$ was found to be sufficiently large for the solution to be independent of d.

The fluid velocity and the temperature gradient along the surface have been calculated from the numerically obtained solution for the streamfunction and the temperature. Then the mean fluid velocity, $\tilde{u}$ and the mean Nusselt number, $\tilde{Nu}$, along the surface were calculated using Simpson's formula.

4. RESULTS AND DISCUSSION

An analytical solution for small times and numerical results obtained using the methods described in Section 3 are presented for the configuration in which the flat surface is vertical or horizontal. It should be noted that analytical and numerical results can also be obtained for different shaped surfaces, such as circular or elliptic cylinders, in a similar way to that described for flat surfaces, namely by taking into account the growth of the thermal boundary-layer at small times.

4.1. *Vertical surface*

Numerical results have been obtained using different grid systems and time steps and the solution was found to be sufficiently accurate when using a grid system of step sizes $\pi/40$ in the x, ξ and $\tilde{y}$ directions and $1/40$ in the η and $\tilde{z}$ directions and a time step $\Delta t = 0.05$. Therefore, unless stated, the numerical results are presented for this discretization.

The mean fluid velocity, $\tilde{u}$ and the mean Nusselt number, $\tilde{Nu}$, along the surface calculated analytically and numerically are presented in Fig. 1 for different values of the Rayleigh number. The analytical and finite-difference results are in very good agreement up to a time which increases as Ra increases, e.g. $t \approx 0.25$ for $Ra = 1$ and $t \approx 1$ for $Ra = 100$ and this is because the dominant term in the analytical expansion of the solution is actually obtained from the boundary-layer equations. However, it is observed that for $Ra \gtrsim 100$ the solution seems to be in the boundary-layer regime, see Fig. 1b and the analytical and numerical solutions are in very good agreement up to $t \approx 1$.

The leading term in the time variation of the mean fluid velocity is obtained by matching the outer flow from the thermal boundary-layer and Fig. 1a shows the importance of matching the inner and outer expansions.

Due to the sudden change of the surface temperature, a thermal boundary-layer is formed at small times adjacent to the surface and streams which flow in opposite directions are generated along the hot and cold regions of the surface. Thus, the flow pattern develops into a row of counter-rotating cells. The heat and flow penetrates further into the porous media as the time or the Rayleigh number increases and the numerical results for $Ra = 1$ and $t \gtrsim 3$ are in very good agreement with the steady-state numerical solution obtained by Bradean *et al.* [3] (see Fig. 1).

Figure 2 presents the streamlines obtained for $Ra = 100$ at different times and shows that at small times the flow separates from the surface at the point of collision of two adjacent boundary-layers, giving rise to two recirculating regions. The separation process can be deduced from the evolution of the fluid velocity and the horizontal temperature gradient at the surface which were calculated at different times as a function of the distance along the surface. The buoyancy force is proportional to the horizontal temperature gradient and at $t \approx 4$ becomes sufficiently strong near the location $x = \pi$ so as to pull the fluid in opposite directions to that of the main flow. The result is that two adjacent counter-rotating recirculating regions are developed in the vicinity of the location $x = \pi$ on the surface and the time at which the flow separates decreases as Ra increases, e.g. $t \approx 4$ for $Ra = 100$ and $t \approx 3$ for $Ra = 300$. The size of the recirculating regions increases as the time of the Rayleigh number increases. However, the magnitude of the buoyancy force near the location $x = \pi$ on the surface decreases in time after the fluid separation, since the magnitude of the fluid velocity increases.

Thus, at small times, the solution seems to develop towards the steady-state patterns as obtained by Bradean *et al.* [3], but at larger values of time small oscillations of the solution are observed in the recirculating regions. As the size of the recirculating regions increases in time, the amplitude of the oscillations increases until there is a complete breakdown of the symmetry in the x direction when the oscillations extend into the main cellular flow. It is found that the point of collision of the two adjacent boundary layers which flow along the surface oscillates about the plane $x = \pi$ and only one recirculating region is developed at the time when the upper or lower cell crosses the plane $x = \pi$. However, as time increases, smaller and smaller recirculating regions are developed. At very large values of time the flow does not separate from the surface (see Fig. 2) and the solution becomes periodic in time.

Figure 3 illustrates the time variation of the mean fluid velocity, $\tilde{u}$ and the mean Nusselt number, $\tilde{Nu}$, is calculated for different grid systems. Very good agreement at small times is obtained between the solutions using $80 \times 80 \times 40$ and $60 \times 60 \times 30$ points in the x, $\tilde{y}$ and $\tilde{z}$ directions, respectively, whereas at very large times there is very good agreement between the period and the amplitude of the oscillations. The only slight dependence of the solution on the grid system is found at moderate values of time and this is due to the breakdown of the symmetry in the x direction at $t \approx 30$. The period of the solutions for the streamfunction and temperature is that for the Nusselt number, namely $p \approx 8.4$. The period of oscillations of the mean fluid velocity, i.e. $p_u \approx 4.2$, is approximately

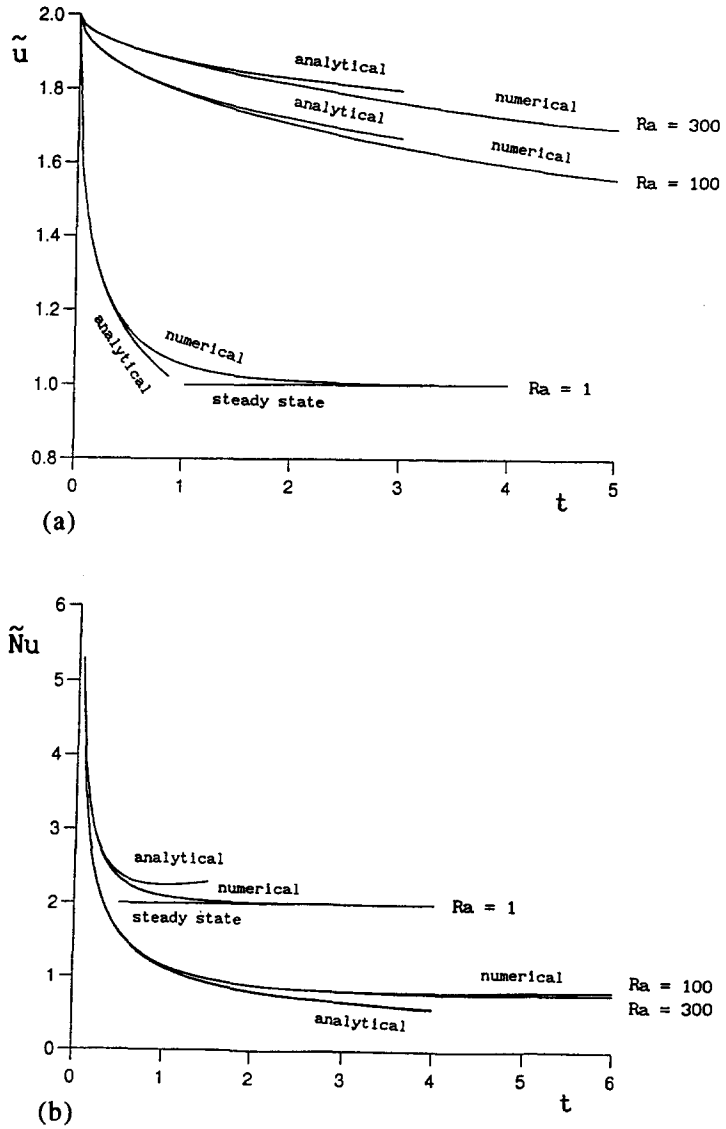

Fig. 1. (a) The mean fluid velocity, $\tilde{u}$ and (b) the mean Nusselt number, $\tilde{Nu}$, calculated analytically and numerically at small times for $Ra = 1$, 100 and 300 and the steady-state values for $Ra = 1$ obtained by Bradean *et al.* [3]. Vertical surface.

half that of the Nusselt number and this is caused by the symmetry of the velocity along the surface, see Fig. 2 which presents the streamlines obtained at $t = 90.30$ and 94.50 whereby the mean fluid velocity reaches two consecutive local minimum values. However, the streamlines and isotherms obtained at $t = 90.30$ and 98.70 are found to be almost indistinguishable.

Hence, the numerical results for $Ra = 100$, as obtained for small and large times, show that the steady-state numerical solution obtained by Bradean *et al.* [3] is not stable. The symmetrical conditions considered in the steady-state situation are only valid up to a time which decreases as the Rayleigh number increases, whereas when using these conditions the unsteady numerical solution for $t \gtrsim 200$ is in very good agreement with the steady-state numerical results (see Fig. 3).

For $Ra \gtrsim 150$ convergent steady-state numerical solutions could not be obtained and it was postulated that the recirculation regions detach from the surface. The evolution of the fluid velocity and the horizontal temperature gradient and, therefore, the buoyancy force along the surface was investigated after the fluid separation. Since the magnitude of the fluid velocity at the surface in the recirculating region increases as the time increases, the buoyancy force near the location $x = \pi$ on the surface acts increasingly against the recirculating flow for $t \gtrsim 8$. Thus, the recirculating regions rotate further from the surface as the time increases, but they do not detach from the surface as predicted in the steady-state problem since the development of the solution described above is changed by small oscillations which occur in the recirculating regions for $t \gtrsim 12$. In Fig. 4 the mean fluid velocity

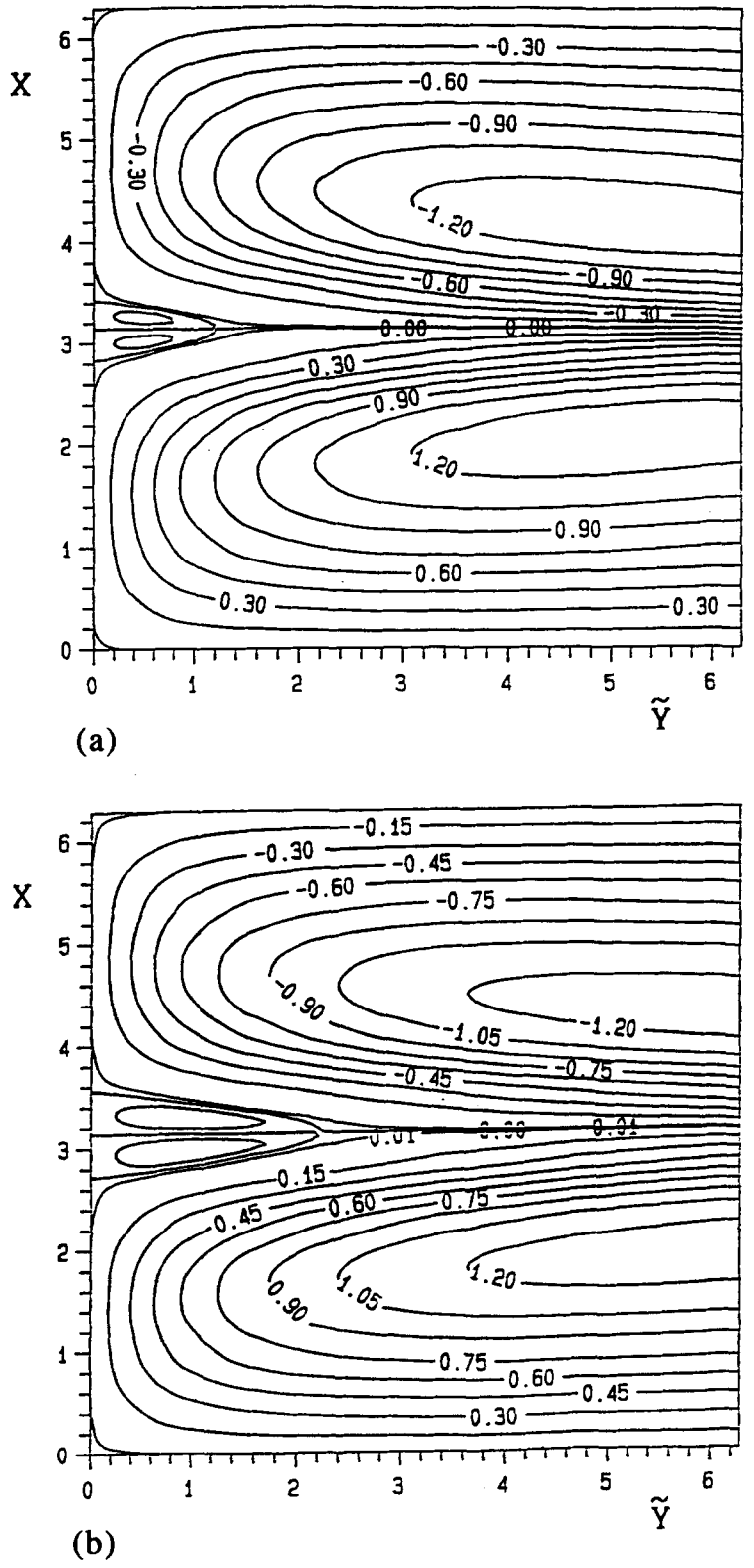

Fig. 2. Streamlines for $Ra = 100$ at (a) $t = 6$, (b) $t = 12$, (c) $t = 90.30$, and (d) $t = 94.50$ in the vertical configuration. (*Continued overleaf.*)

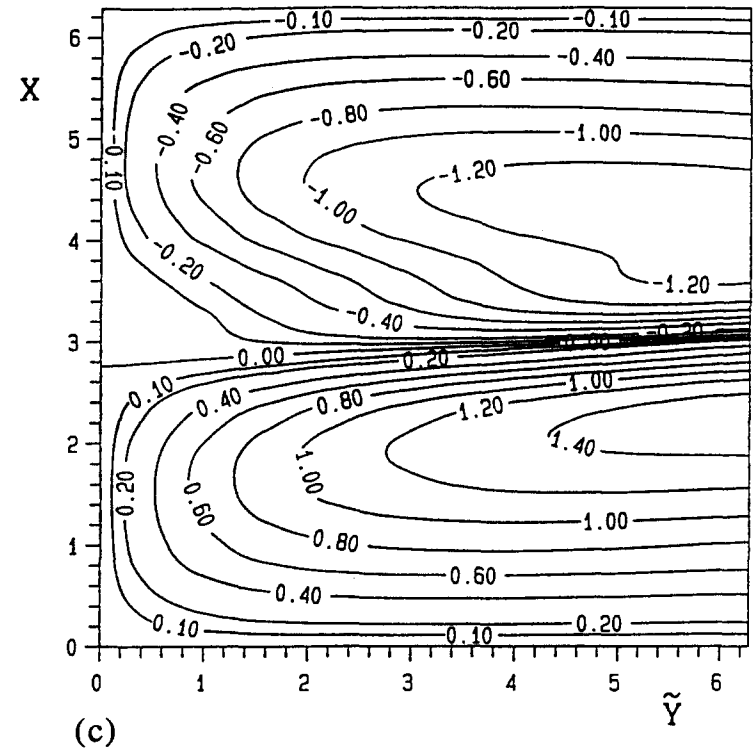

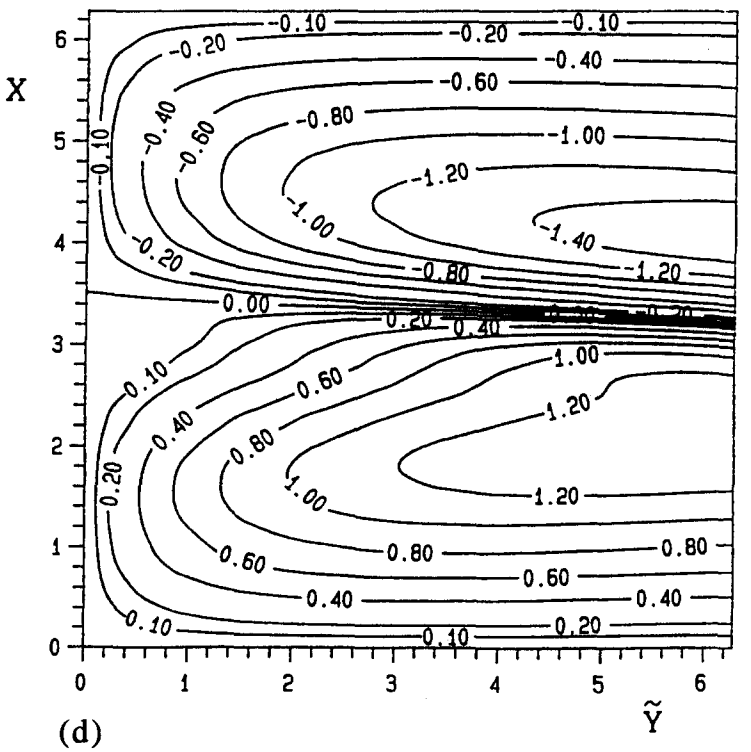

Fig. 2. *Continued.*

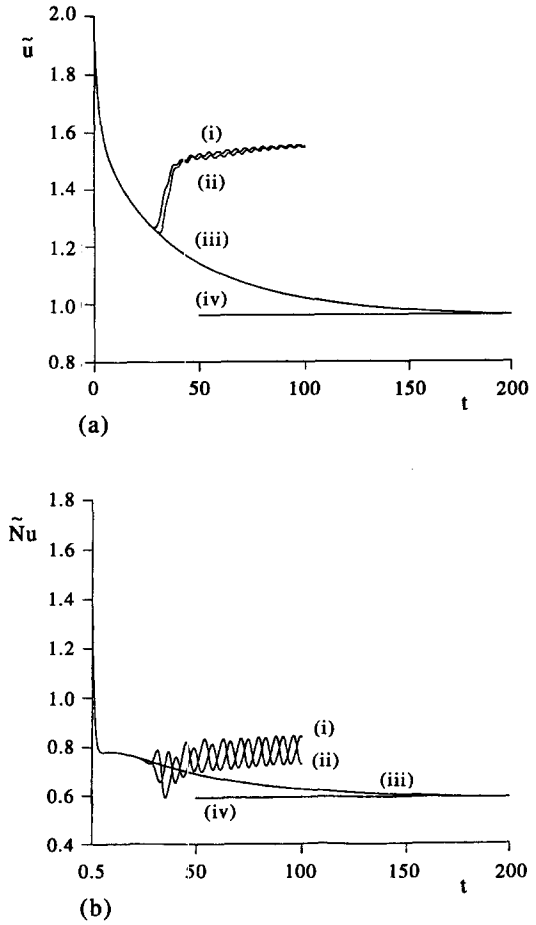

Fig. 3. (a) The mean fluid velocity, $\tilde{u}$ and (b) the mean Nusselt number, $\tilde{Nu}$, as a function of time for $Ra = 100$ calculated using (i) $80 \times 80 \times 40$, (ii) $60 \times 60 \times 30$ points in the x, $\tilde{y}$ and $\tilde{z}$ directions, respectively, (iii) the additional symmetrical conditions and (iv) the steady state as obtained by Bradean *et al.* [3]. Vertical surface.

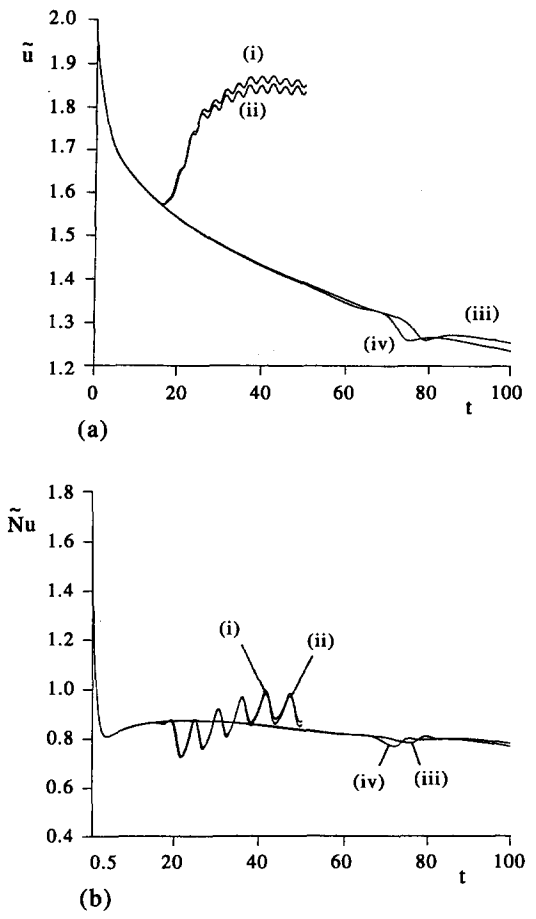

Fig. 4. (a) The mean fluid velocity, $\tilde{u}$ and (b) the mean Nusselt number, $\tilde{Nu}$, as a function of time for $Ra = 300$ calculated using (i) $80 \times 80 \times 40$, (ii) $60 \times 60 \times 30$ points in the x, $\tilde{y}$ and $\tilde{z}$ directions, respectively, and assuming the additional symmetrical conditions and using the grid systems, (iii) $40 \times 80 \times 40$ and (iv) $30 \times 60 \times 30$. Vertical surface.

and the mean Nusselt number are plotted against the time as calculated for different grid systems and using the additional symmetrical conditions considered in the steady-state and show that up to $t \approx 17$ these conditions are satisfied by the numerical solution which eventually becomes periodic in time. As the Rayleigh number increases the period of the solution for the streamfunction and temperature, which is the period of oscillations of the Nusselt number, decreases, i.e. $p \approx 5.6$ for $Ra = 300$. However, the amplitude of oscillations of the mean fluid velocity increases as Ra increases, whereas the amplitude of the Nusselt number seems to be independent of the Rayleigh number and the values calculated for $Ra = 100$ and 300 agree within 2%.

Figure 5 presents the streamlines for $Ra = 300$ at $t = 50$ and 52.8. It shows that now the flow separates at large times when the solution is almost periodic in time and a recirculating region is developed at a time near the point of collision of the two adjacent boundary layers which flow along the surface.

The additional symmetrical conditions assumed in the steady-state situation are now considered for $Ra = 300$ in order to check whether, in the absence of the instability in the x direction, the recirculating region developed at small times near the location $x = \pi$ on the surface detach from the surface as predicted by Bradean *et al.* [3]. Without the interference of the oscillations in the recirculating region, the buoyancy force now acts increasingly against the recirculating flow up to $t \approx 40$, when it becomes sufficiently strong so as to pull the fluid in the opposite direction to that of the recirculating flow. The result is that a second recirculating region, which increases in size as the time increases, develops as the first recirculating region detaches from the surface, see Fig. 5 where the streamlines are presented at $t = 50$ and 80.

However, the second recirculating region is consumed by the main cell when the first recirculating region has completely detached from the surface and this is because it rotates in the direction of the main cell. Then a third recirculating region develops in a

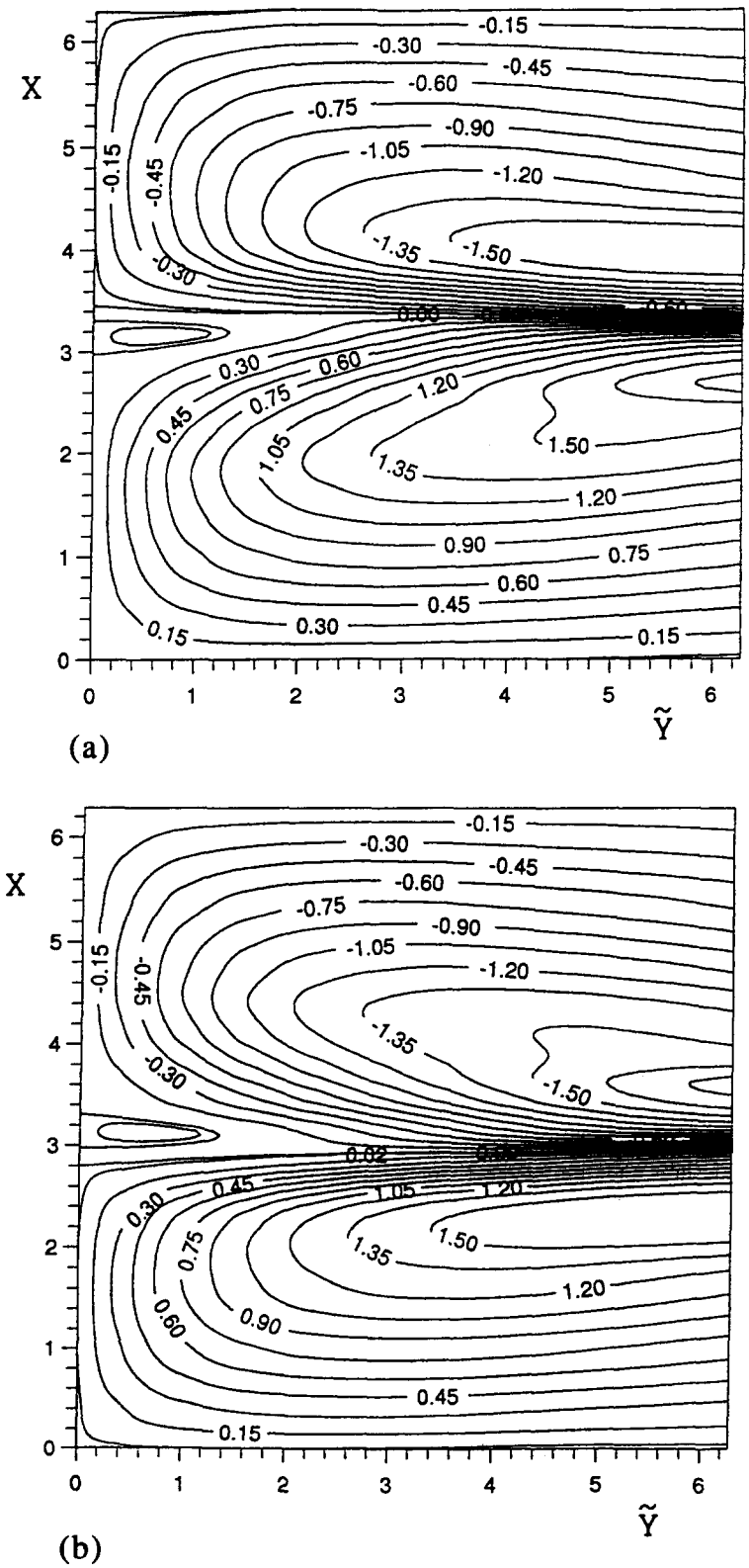

Fig. 5. Streamlines for $Ra = 300$ obtained at (a) $t = 50$ and (b) $t = 52.8$ and using the additional symmetrical conditions and at (c) $t = 50$ and (d) $t = 80$ in the vertical configuration. (*Continued opposite.*)

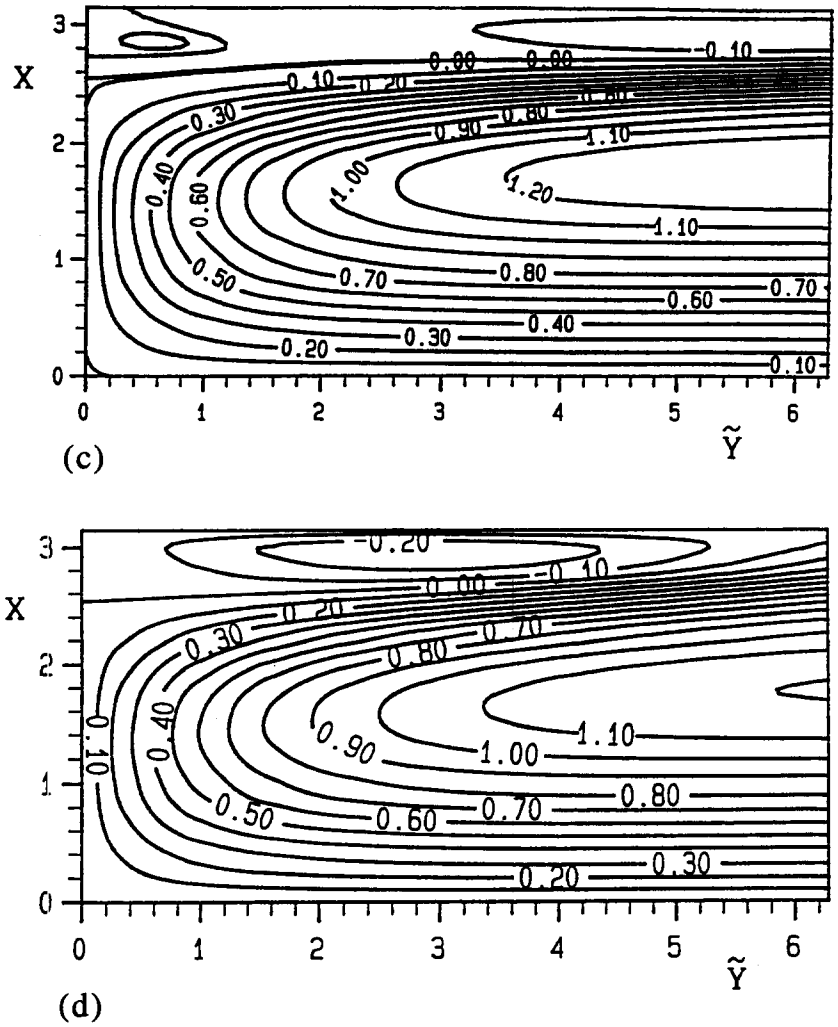

Fig. 5. *Continued.*

similar way to that described at small times for the first recirculating region and this rotates in the opposite direction to that of the main cell (see Fig. 5d). This evolution of the solution is repeated until a recirculating flow region stabilizes near the surface. At very large times the solution oscillates in time in the recirculating region which does not detach from the surface and eventually becomes periodic in time.

The mean fluid velocity $\tilde{u}$ and the mean Nusselt number, $\tilde{Nu}$, as a function of time presented in Fig. 6 shows that in this situation the solution at large times is more dependent on the grid system than is the solution obtained in the domain $\tilde{D}$. The number of recirculating regions that detach from the surface depends on the mesh size. However, at very large times, the period and the amplitude of the oscillations do not depend on the grid system provided that the step sizes are sufficiently small.

The period of the streamfunction and temperature solutions is again the same as the period of oscillations of the Nusselt number, namely $p \approx 11.35$ and the streamlines and isotherms obtained at $t = 251$ and 262.35, at which the Nusselt number reaches two consecutive local minimum values, are found to be almost indistinguishable.

4.2. *Horizontal surface*

An investigation of numerical results obtained for different grid systems and time steps showed that the numerical solution is sufficiently accurate when using 80 points in the x, ξ and $\tilde{y}$ directions and a time step $\Delta t = 0.05$. The number of points in the η and $\tilde{z}$ directions is taken to be dependent on the Rayleigh number and 40, 80 and 120 points are chosen for $Ra = 10/\pi$, $100/\pi$ and $200/\pi$, respectively, in order to obtain the solution at very large values of y. However, using a different mesh size in the η and $\tilde{z}$ directions does not influence the solution in the domain $\tilde{D}$ and, therefore, the numerical results presented for this configuration have been obtained using the above discretizations.

Figure 7 presents the mean fluid velocity, $\tilde{u}$ and the mean Nusselt number, $\tilde{Nu}$, along the surface at small times and shows very good agreement between the

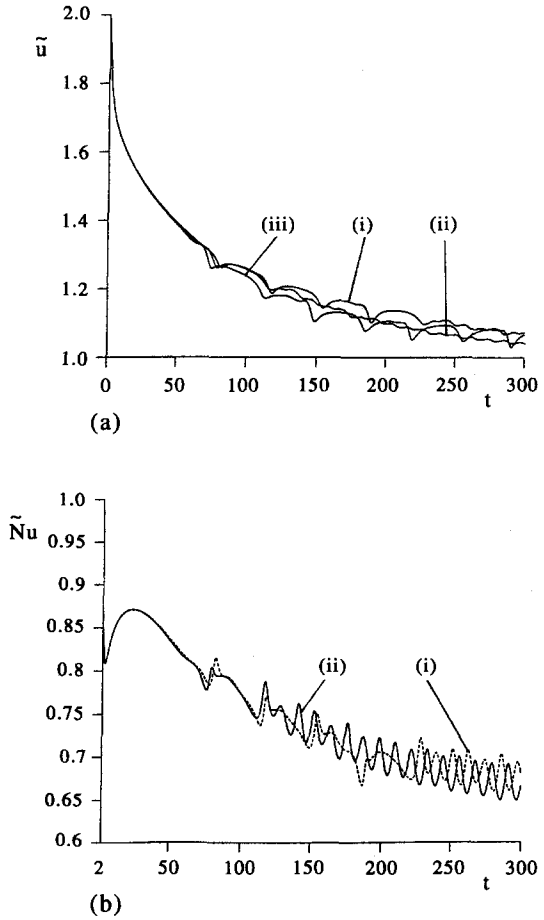

Fig. 6. (a) The mean fluid velocity, $\tilde{u}$ and (b) the mean Nusselt number, $\tilde{Nu}$, as a function of time for $Ra = 300$ obtained using the additional symmetrical conditions and the grid systems (i) $50 \times 100 \times 50$, (ii) $40 \times 80 \times 40$, and (iii) $30 \times 60 \times 30$ points in the x, $\tilde{y}$ and $\tilde{z}$ directions, respectively. Vertical surface.

analytical and numerical results up to a time which increases as the Rayleigh number increases, i.e. up to $t \approx 0.5$ for $Ra = 10/\pi$ and $t \approx 3$ for $Ra = 200/\pi$. As time increases the magnitude of the mean fluid velocity increases from $\tilde{u} = 0$ at $t = 0$ whereas in the situation when the surface is vertical the mean fluid velocity impulsively increases up to $\tilde{u} = 2$ at $t = 0$ and then decreases in time. The values of the mean Nusselt number calculated at small times for $Ra = 100$ and $200/\pi$ indicate that the boundary-layer regime is approached at $Ra \approx 200/\pi$ (see Fig. 7b). It should be noted that the boundary-layer scalings with the Rayleigh number at small times and the steady-state do not coincide and this was also obtained by Pop *et al.* [11].

The streamlines and isotherms for $Ra = 10/\pi$, $100/\pi$ and $200/\pi$ and at different times are plotted in Fig. 8 and show that the heated and cooled horizontal surface generates streams which flow between the cold and hot regions of the surface, giving rise to a cellular flow. Initially, both the heat and flow penetrate to larger distances into the porous media as time increases. However, the height of the cellular flow penetration reaches a maximum value at a large time, which increases as the Rayleigh number increases and then slowly decreases towards the steady-state value obtained by Bradean *et al.* [6]. For small values of the Rayleigh number, i.e. $Ra = 10/\pi$, the height to which the flow penetrates into the porous media remains almost constant at very large times since its maximum value is approximately the steady-state value and the streamlines obtained at $t = 200$ (see Fig. 8) and the steady-state are found to be almost indistinguishable. As Ra increases the maximum height of the cellular flow increases, whereas the height of the steady-state flow slightly decreases, see Bradean *et al.* [6] and Fig. 8 shows the streamlines and isotherms for $Ra = 100/\pi$ at $t = 300$ and 2000. It is interesting to note that the shape of the streamline and isotherm patterns obtained at $t = 300$, when the height of the cellular flow reaches its maximum value, is similar to those obtained by Poulikakos and Bejan [5] in the steady-state problem using a prescribed temperature boundary condition at a large but finite distance from the surface. However, Bradean *et al.* [6] showed that this boundary condition cannot be enforced in the steady-state problem since the heat penetrates infinitely into the porous media and the temperature at infinity depends on the Rayleigh number. For $t \gtrsim 800$ the height of the cellular flow very slowly decreases towards the steady-state value obtained by Bradean *et al.* [6] and at $t = 2000$ the streamlines near the surface are similar to the steady-state patterns. For larger values of the Rayleigh number the maximum height of the cellular flow is very large and numerical results have been obtained only up to $Ra = 200/\pi$. For $Ra = 200/\pi$ the evolution of the solution is similar to that described for $Ra = 100/\pi$ but the time at which the solution becomes comparable with the steady-state solution is too large and numerical results have been obtained only up to $t = 2000$, see the streamlines and isotherms plotted in Fig. 8. However, the numerical results show that the flow does not separate from the horizontal surface at the point of collision of two boundary layers.

Since the hot fluid rises and the cold fluid is trapped near the surface the temperature of one cell becomes hotter as the time or the Rayleigh number increases and at large times above the cellular flow the heat is transferred by conduction to infinity. In order to investigate the penetration of heat into the porous media, the temperature as a function of y at $x = 0$ and π for $Ra = 10/\pi$ is plotted in Fig. 9. At large times, the temperature above the cellular flow does not depend on x and decreases from a positive value to zero at infinity. As time increases the solution very slowly develops towards the steady-state solution obtained by Bradean *et al.* [6]. However, a steady-state solution of similar shape to that obtained at $t = 200$ which satisfies $T \to 0$ as $y \to \infty$ is not possible since the heat conduction equation has to be satisfied

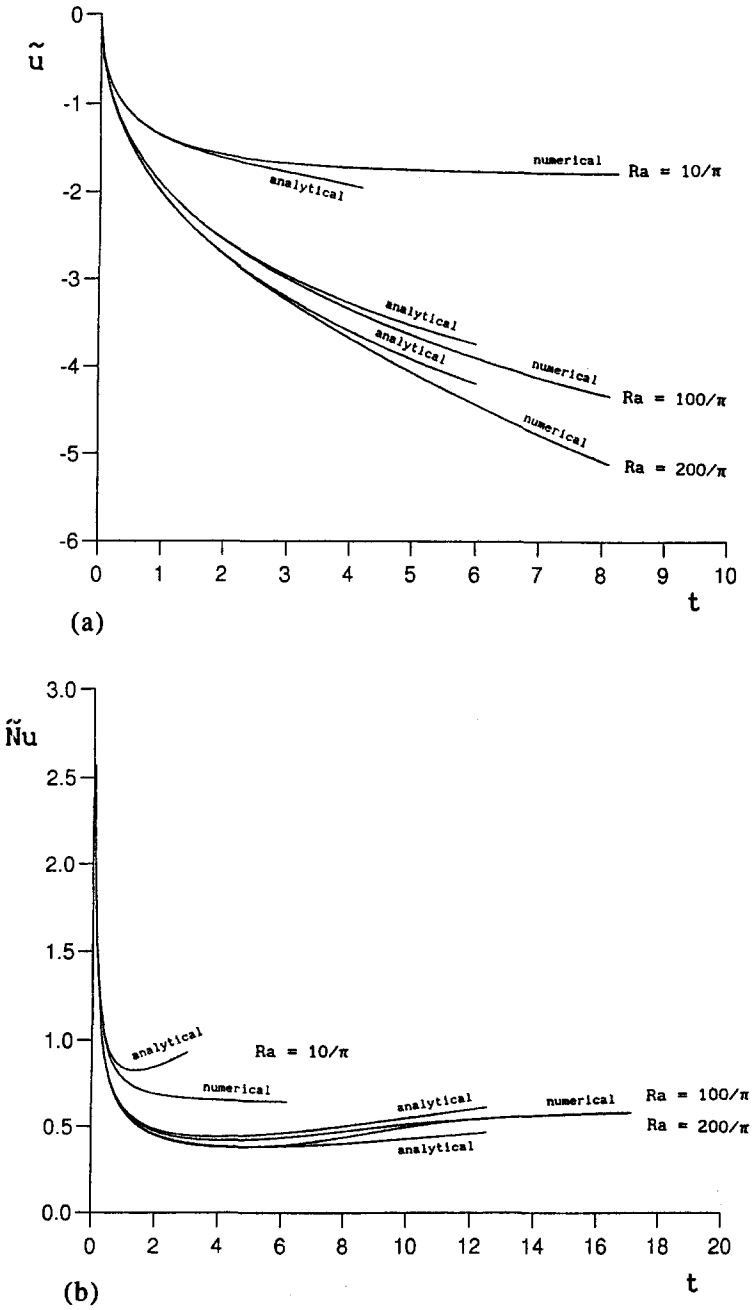

Fig. 7. (a) The mean fluid velocity, $\tilde{u}$, and (b) the mean Nusselt number, $\tilde{Nu}$, calculated analytically and numerically at small times for $Ra = 10/\pi$, $100/\pi$ and $200/\pi$ in the horizontal configuration.

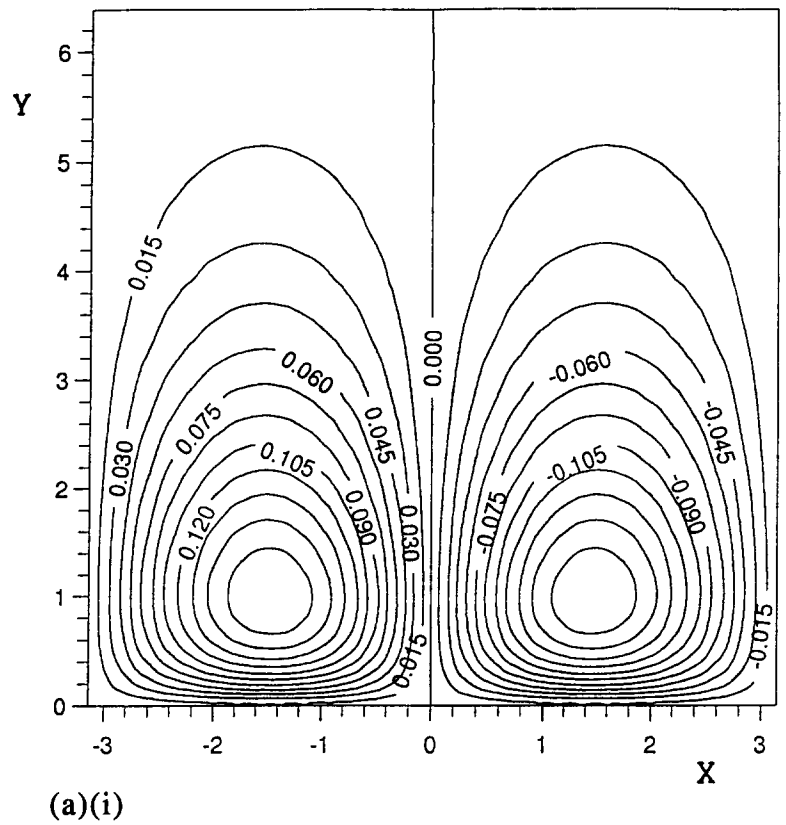

(a)(i)

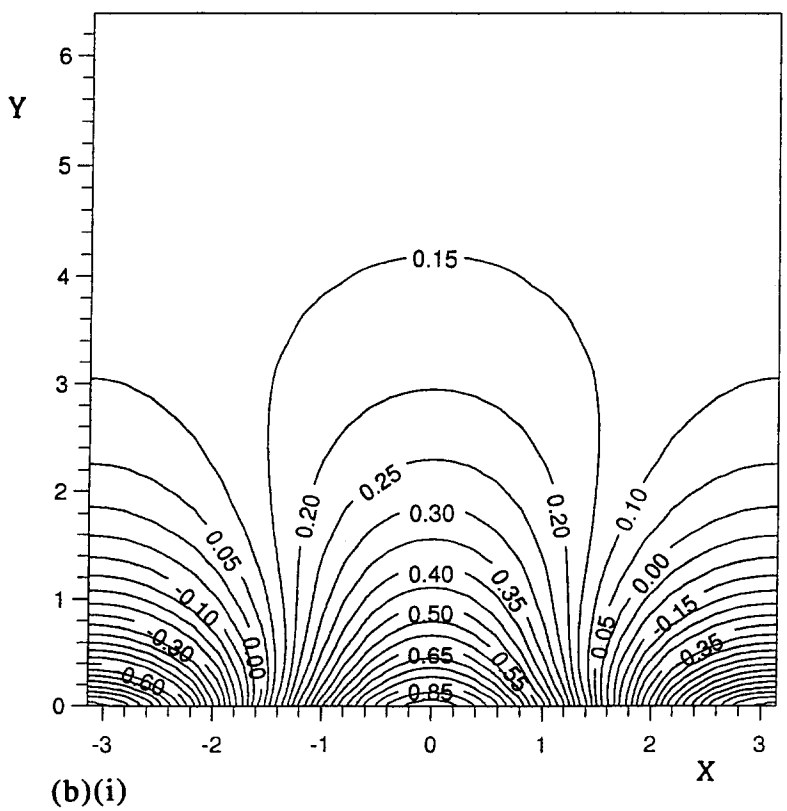

(b)(i)

Fig. 8. (a) Streamlines and (b) isotherms for (i) $Ra = 10/\pi$ at $t = 200$, (ii), (iii) $Ra = 100/\pi$ at $t = 300$ and 2000, respectively, and (iv) $Ra = 200/\pi$ at $t = 2000$ in the horizontal configuration. (*Continued opposite and overleaf.*)

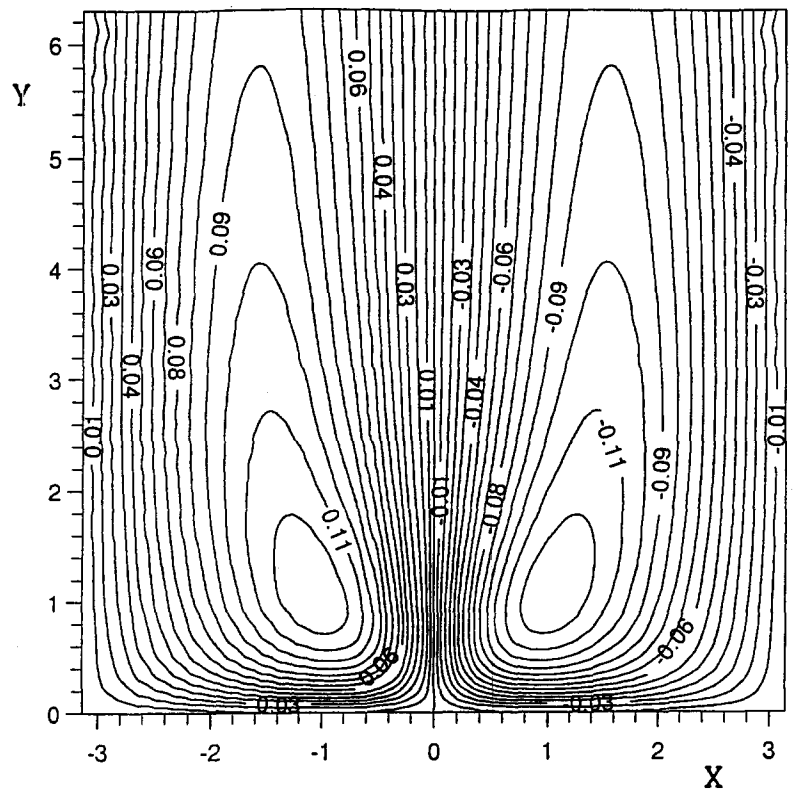

(a)(ii)

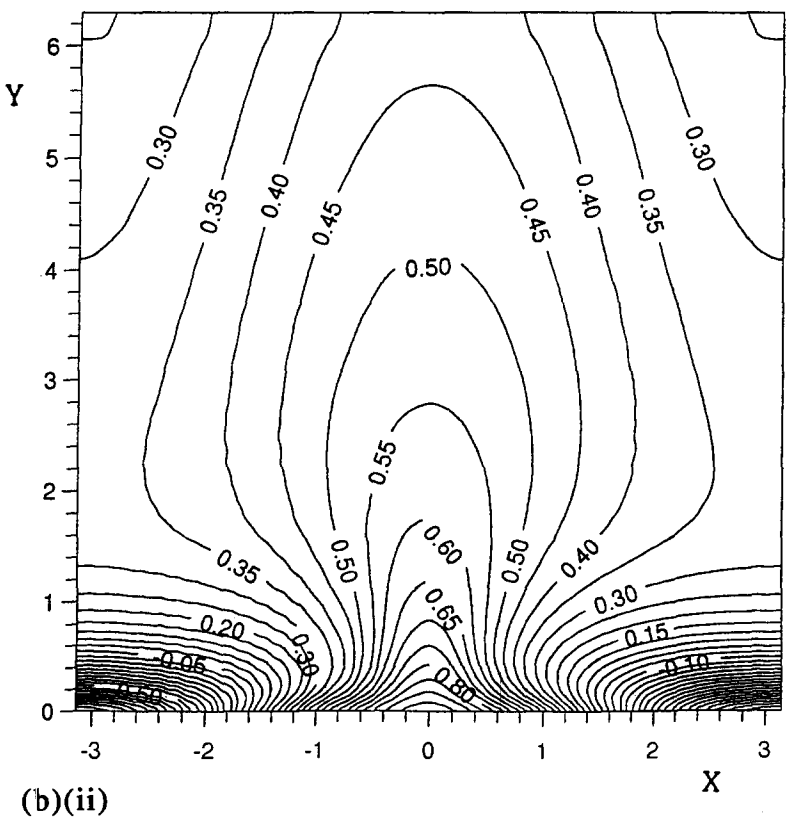

(b)(ii)

Fig. 8. *Continued.*

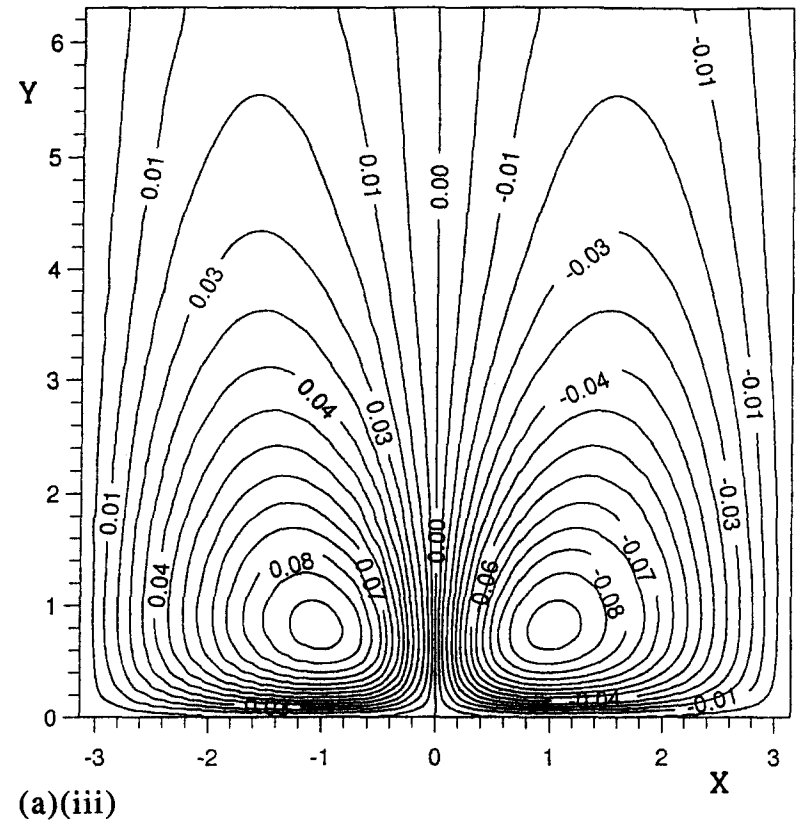

(a)(iii)

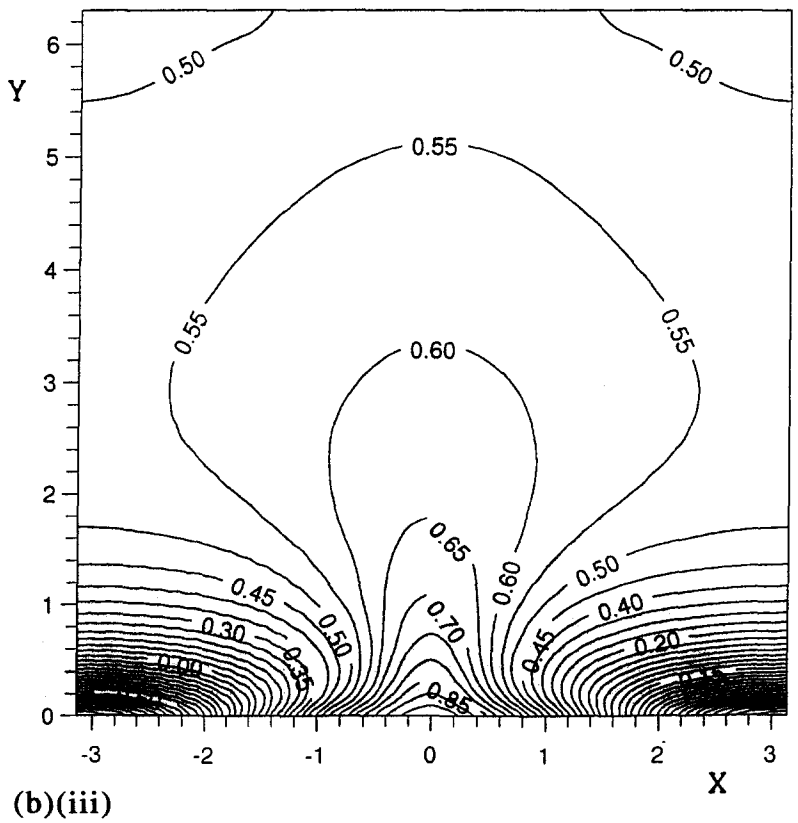

(b)(iii)

Fig. 8. *Continued.*

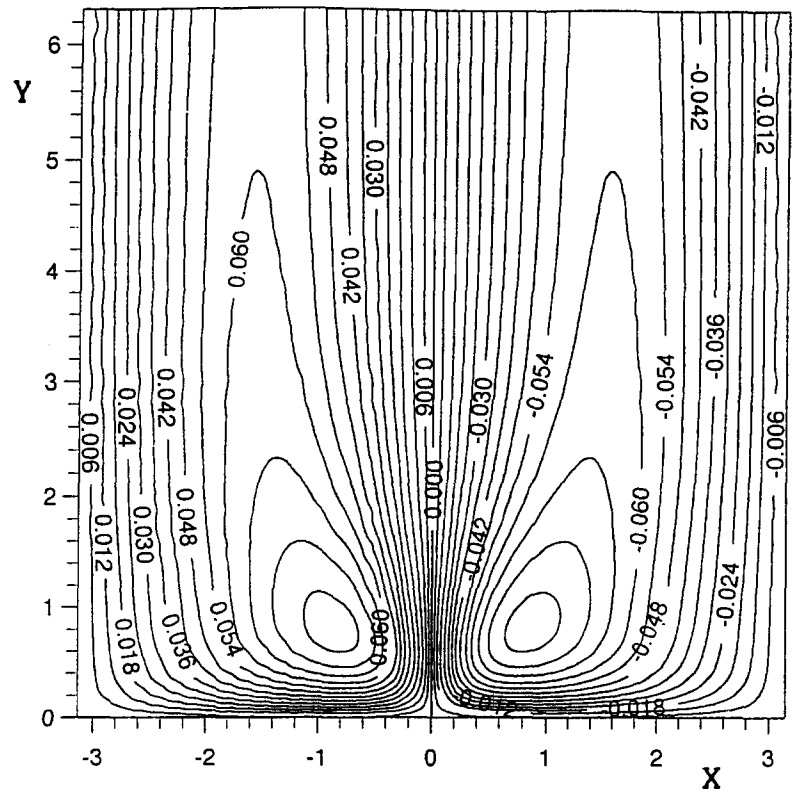

(a)(iv)

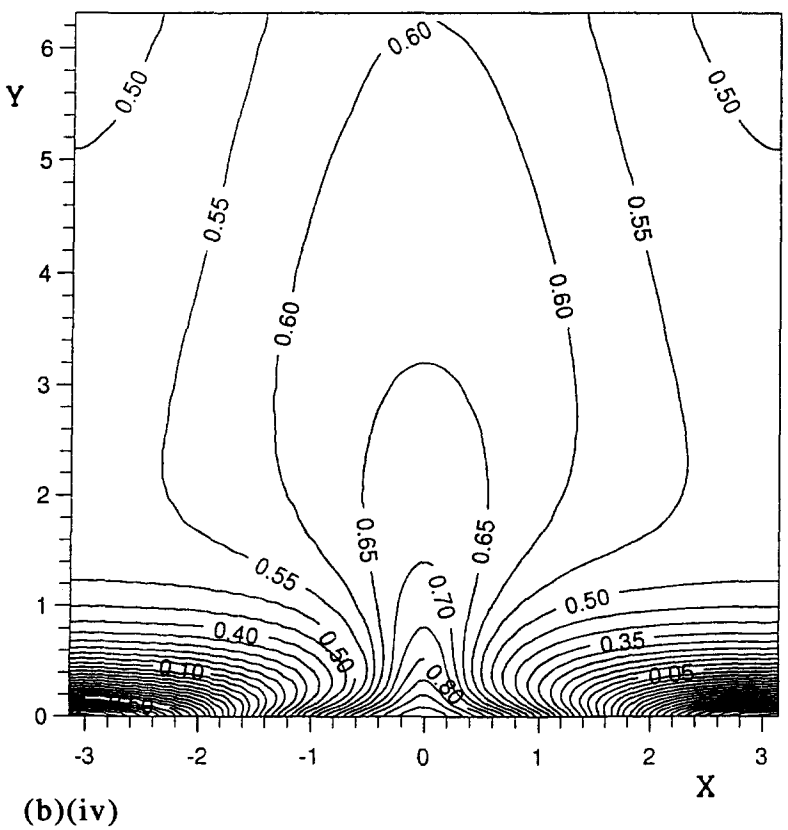

(b)(iv)

Fig. 8. *Continued.*

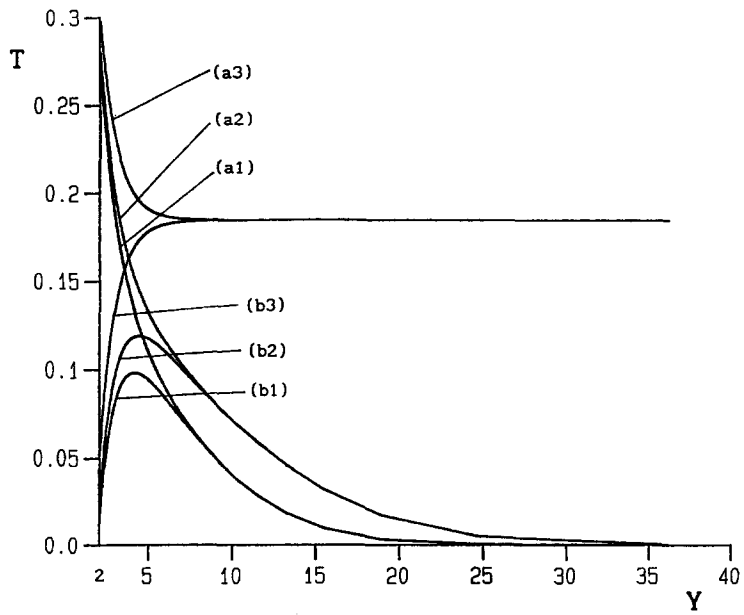

Fig. 9. The temperature as a function of y at the locations (a) $x = 0$ and (b) $x = \pi$ calculated for $Ra = 10/\pi$ at (1) $t = 100$, (2) $t = 200$ and, (3) the steady state as obtained by Bradean *et al.* [6]. Horizontal surface.

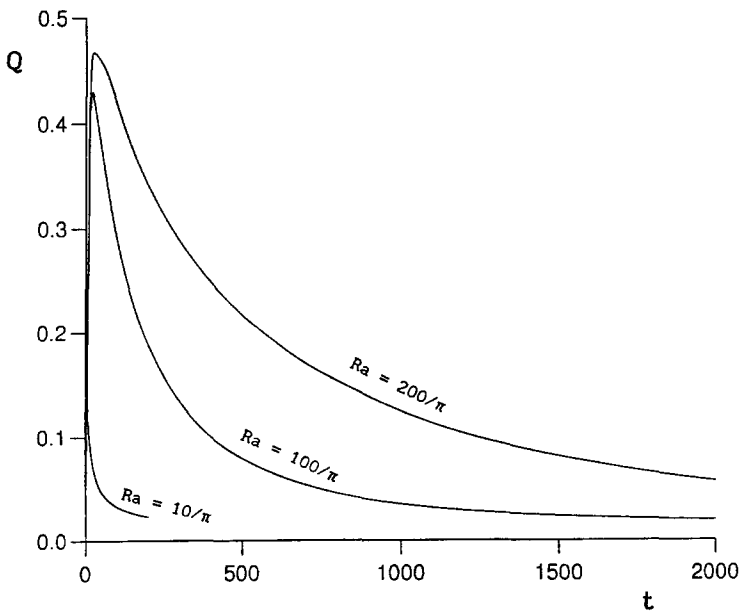

Fig. 10. The average heat flux at the surface, Q, as a function of time calculated for $Ra = 10/\pi$, $100/\pi$ and $200/\pi$ in the horizontal configuration.

Table 1. The mean velocity, $\tilde{u}$ and the mean Nusselt number, $\tilde{N}u$, along the horizontal surface for (a) $Ra = 10/\pi$ and (b) $Ra = 100$ and $200/\pi$ calculated at large times and the steady-state values obtained by Bradean *et al.* [6]

(a)

t	$\tilde{u}$	$\tilde{N}u$
50	−1.761	0.607
100	−1.756	0.601
150	−1.754	0.598
200	−1.753	0.597
∞	−1.745	0.587

(b)

	$Ra = 100/\pi$		$Ra = 200/\pi$	
t	$\tilde{u}$	$\tilde{N}u$	$\tilde{u}$	$\tilde{N}u$
500	−4.211	0.394	−5.366	0.452
1000	−4.104	0.369	−5.139	0.399
1500	−4.074	0.362	−5.020	0.372
2000	−4.063	0.359	−4.949	0.357
∞	−4.006	0.346	−4.755	0.318

Table 2. The temperature at the location $x = 0$ and $y = 1.80$ for $Ra = 100/\pi$ and at different times calculated (A) using equation (76) and (N) numerically

	$T(0,1.80)$	
t	A	N
50	0.289	0.292
100	0.301	0.302

above the cellular flow and the solution is a constant temperature which depends on the Rayleigh number.

The average heat flux at the surface

$$Q = \int_0^{\pi} (-\partial T/\partial \tilde{y})_{y=0}\, dx \tag{73}$$

as a function of time for different values of Ra is plotted in Fig. 10 and shows that, unlike the vertical configuration when the average heat flux at the surface is zero at all times, more heat enters than leaves the porous media and, therefore, heat enters the porous media at all times. This is the reason behind the infinite heat penetration. However, at very large values of time, the average heat flux at the surface slowly decreases towards zero and this is consistent with the steady-state solution.

Table 1 presents the values of the mean fluid velocity, $\tilde{u}$ and the mean Nusselt number, $\tilde{N}u$, along the surface for $Ra = 10/\pi$, $100/\pi$ and $200/\pi$ at progressively increasing values of time and a slow approach to the steady-state values is apparent. Since the heat penetrates infinitely into the porous media, the steady-state temperature for $Ra = 10/\pi$ is compared at different distances from the surface with the temperature at large times in Fig. 11. It is obtained that the steady-state is approached at larger values of time as the distance from the surface increases and this is due to the fact that the average heat flux at the surface tends to zero as $t \to \infty$. However, the numerical results obtained at large times indicate that the solution decays algebraically to the steady-state solution. An empirical expression of the solution at very large times can be obtained at any point in the solution domain by assuming that

$$T(x,y) = T_{\infty}(x,y) + T_{-1}(x,y)t^{-p_1(x,y)} \tag{74}$$

$$\psi(x,y) = \psi_{\infty}(x,y) + \psi_{-1}(x,y)t^{-q_1(x,y)} \tag{75}$$

where T_{∞} and ψ_{∞} are the steady-state solution and T_{-1}, p_1, ψ_{-1} and q_1 are calculated at a point (x,y) in the solution domain using the numerical results obtained at two different very large times. For example, for $Ra = 10/\pi$ equation (74) is determined at the location $x = 0$ and $y = 1.80$ using the numerical solution obtained at $t = 150$, 200 and the steady-state, namely

$$T = 0.326 - 0.341t^{-0.566} \tag{76}$$

and Table 2 shows that there is good agreement between this equation and the numerical results. However, further analytical study is required in order to obtain expansions of the solution in terms of the large time.

5. CONCLUSION

The analytical and numerical results are found to be in very good agreement at small times and show that near the heated and cooled flat surface the flow consists of a row of counter-rotating cells, each cell developing along either the hot or cold regions of the vertical surface and between the cold and hot regions of the horizontal surface.

In the vertical configuration the heat and flow penetrate further into the porous media as the time or Rayleigh number increases. For $Ra \gtrsim 40$ and at small times the flow separates from the surface and the solution appears to develop towards the steady-state. However, the additional symmetrical conditions assumed in the steady-state situation are only satisfied up to a time which decreases as Ra increases and at very large times the solution is periodic in time. A recirculating flow region develops at a time near the point of collision of two boundary layers which flow along the vertical surface, provided that the Rayleigh number is sufficiently large.

When the surface is horizontal the cellular flow initially penetrates further into the porous media and the temperature of one cell becomes hotter as time or Rayleigh number increases. However, at very large times, the height of the flow penetration decreases to its steady-state value whereas the heat above the cellular flow is transferred by conduction to infinity. The greater the distance from the surface the later is the steady-state approached. Unlike the vertical configuration, the flow does not separate from the hori-

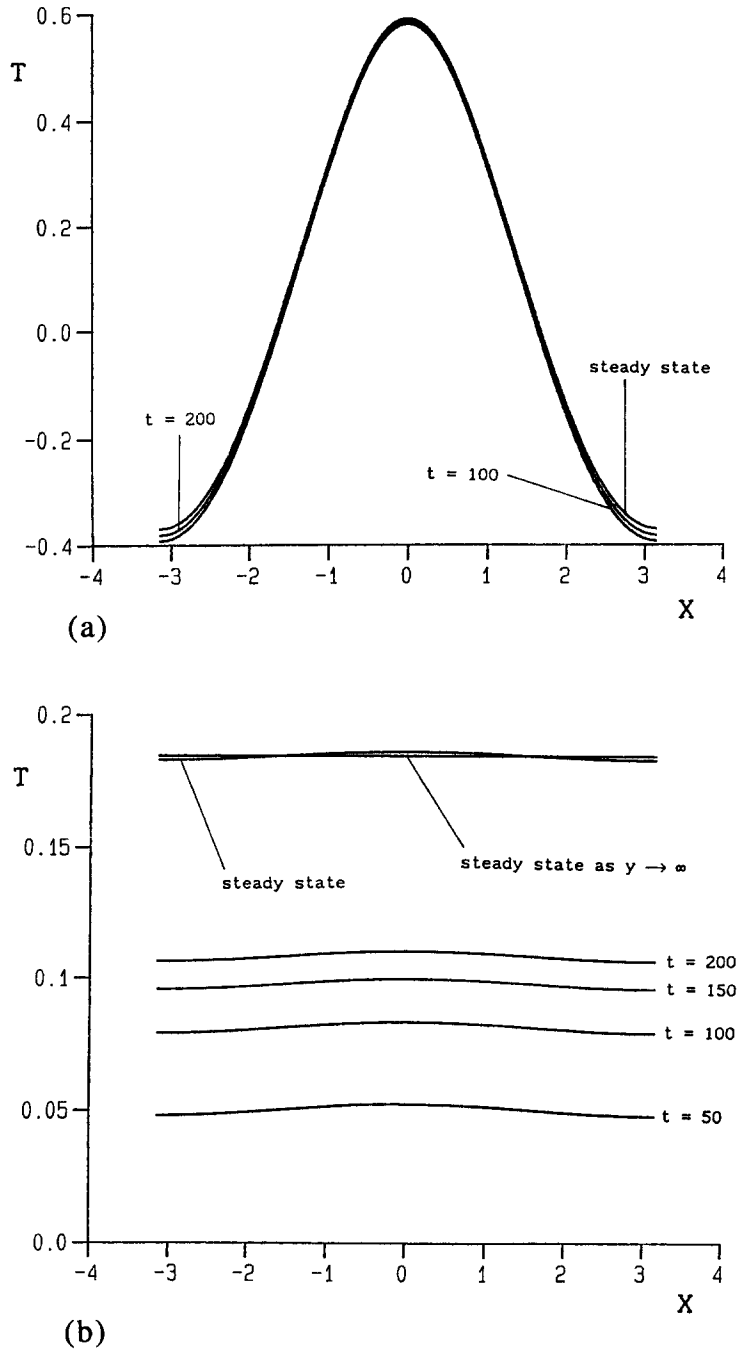

Fig. 11. The temperature as a function of x at the locations (a) $y = 0.70$ and (b) $y = 6.38$ calculated for $Ra = 10/\pi$ at different times in the horizontal configuration.

zontal surface at the point of collision of two boundary layers.

REFERENCES

1. Cheng, P., Heat transfer in geothermal systems. *Advances in Heat Transfer*, 1978, **14**, 1–105.
2. Nield, D. A. and Bejan, A., *Convection in Porous Media*. Springer, New York, 1992.
3. Bradean, R., Ingham, D. B., Jeggs, P. J. and Pop, I., Free convection fluid flow due to a periodically heated and cooled vertical flat plate embedded in a porous media. *International Journal of Heat and Mass Transfer*, 1996, **39**, 2545–2557.
4. Smith, F. T. and Duck, P. W., Separation of jets or thermal boundary layers from a wall. *Quarterly Journal of Mechanics and Applied Mathematics*, 1977, **30**, 143–156.
5. Poulikakos, D. and Bejan, A., Penetrative convection in porous medium bounded by a horizontal wall with hot and cold spots. *International Journal of Heat and Mass Transfer*, 1984, **27**, 1749–1757.
6. Bradean, R., Ingham, D. B., Heggs, P. J. and Pop, I., Buoyancy-induced flow adjacent to a periodically heated and cooled horizontal surface in a porous media. *International Journal of Heat and Mass Transfer*, 1996, **39**, 615–630.
7. Ingham, D. B., Merkin, J. H. and Pop, I., The collision of free convection boundary layers on a horizontal cylinder embedded in a porous medium. *Quarterly Journal of Mechanics and Applied Mathematics*, 1983, **36**, 313–335.
8. Wang, C.-Y., The flow past a circular cylinder which is started impulsively from rest. *Journal of Mathematics and Physics*, 1967, **46**, 195–202.
9. Wang, C.-Y., Separation and stall of an impulsively started elliptic cylinder. *Journal of Applied Mechanics*, 1967, **34**, 823–828.
10. Pop, I., Ingham, D. B. and Cheng, P., Transient free convection about a horizontal circular cylinder in a porous medium. *Fluid Dynamics Research*, 1993, **12**, 295–305.
11. Pop, I., Ingham, D. B. and Bradean, R., Transient free convection about a horizontal circular cylinder in a porous medium with constant surface flux heating. *Acta Mechanica*.
12. Collins, W. M. and Dennis, S. C. R., The initial flow past an impulsively started circular cylinder. *Quarterly Journal of Mechanic and Applied Mathematics*, 1971, **26**, 53–75.
13. Ingham, D. B., Merkin, J. H. and Pop, I., Flow past a suddenly cooled vertical flat surface in a saturated porous medium. *International Journal of Heat and Mass Transfer*, 1982, **25**, 1916–1919.
14. Ingham, D. B. and Brown, S. N., Flow past a suddenly heated vertical plate in a porous medium. *Proceedings of the Royal Society of London*, 1986, **A403**, 51–80.
15. Bradean, R., Ingham, D. B., Heggs, P. J. and Pop, I., The penetration of unsteady free convection from a heated and cooled vertical flat surface in a porous media. *The Proceedings of the Symposium on Thermal Science and Engineering in Honor of Chancellor Chang Lin-Tien*, Berkeley, CA (in press).
16. Bradean, R., Ingham, D. B., Heggs, P. J. and Pop, I., Unsteady free convection from a horizontal surface embedded in a porous media. *The Proceedings of the 2nd European Thermal Sciences and 14th UIT National Heat Transfer Conference* Rome, Italy (submitted).